

Influence of incorporation of Al³⁺ ions on the structural, optical and AC impedance characteristics of spin coated ZnO thin films

L. Suganya · B. Sundaresan · G. Sankareswari ·
K. Ravichandran · B. Sakthivel

Received: 11 October 2013 / Accepted: 5 November 2013 / Published online: 19 November 2013
© Springer Science+Business Media New York 2013

Abstract Aluminium doped zinc oxide thin films were deposited onto glass substrate using spin coating technique. The effects of Al doping on structural, optical and electrical properties of these films were investigated. X-ray diffraction analysis showed that all the thin films were of polycrystalline hexagonal wurtzite structure with (002) as preferential orientation except 2 at.% of Al doped ZnO films. The optical band gap was found to be 3.25 eV for pure ZnO film. It increases up to 1.5 at.% of Al doping (3.47 eV) and then decreased slightly for the doping level of 2 at.% (3.42 eV). The reason for this widening of the optical band gap up to 1.5 at.% is well described by Burstein–Moss effect. The photoluminescence spectra of the films showed that the blue shift and red shift of violet emission were due to the change in the radiative centre between zinc vacancy and zinc interstitial. Variation in ZnO grain boundary resistance against the doping concentration was observed through AC impedance study.

1 Introduction

Transparent conducting oxide (TCO) films are promising owing to their wide variety of technological applications [1]. ZnO, one of such TCOs, has gained great attention from

researchers due to its superior properties and suitability for use in photovoltaic cells and many other opto-electronic devices. It is an n-type direct band gap semiconductor having a wide band gap (3.37 eV) and high exciton binding energy (60 meV) [2]. Indium tin oxide (ITO) and tin oxide (SnO₂) have long been established and used as transparent conducting materials in many applications. Recently, ZnO has been considered as a potential substitute for ITO and SnO₂, owing to a number of encouraging advantages like low cost, non-toxicity and stability in the presence of hydrogen plasma [3, 4]. ZnO thin films found potential applications in making flat panel liquid crystal displays, antibacterial agents, gas sensors, varistors, photo catalysts, solar cells and transparent conducting electrodes [5–10]. These applications are achieved by doping with specific elements. Doping is an effective method to tune the optical, electrical and magnetic properties of ZnO for practical applications. Group III elements such as aluminium has been doped into ZnO with the aim to enhance its properties towards the fabrication of ZnO based light emitters. But still many of its properties are to be tuned to achieve the fabrication of effective optoelectronic devices based on aluminium doped zinc oxide (AZO–ZnO:Al) thin films.

Aluminium doped zinc oxide (AZO) thin films have been prepared using various techniques such as magnetron sputtering [11], pulsed laser deposition [12], SILAR [13], spray pyrolysis [14], sol–gel [15] and so on. Among these techniques, the sol–gel method using spin coater is popular due to its simplicity, safety and low cost. Moreover, it is easy to realize dopant incorporation and large area coating.

In the present work, ZnO thin films are deposited with different concentrations of aluminium using spin coating technique. The structural, optical and electrical properties of the prepared thin films are studied through X-ray diffractometry (XRD), UV-vis-NIR spectrophotometry, spectrofluorometry and AC impedance technique techniques and are reported.

L. Suganya · B. Sundaresan · G. Sankareswari
Centre for Research and Post Graduate Studies in Physics, Ayya Nadar Janaki Ammal College (Autonomous), Sivakasi 626 124, Tamil Nadu, India

K. Ravichandran (✉) · B. Sakthivel
Post Graduate and Research Department of Physics, AVVM Sri Pushpam College (Autonomous), Poondi, Thanjavur 613 503, Tamil Nadu, India
e-mail: kkr1365@yahoo.com; kkravi1365@gmail.com

2 Experimental details

2.1 Materials

AR/BDH grade chemicals, zinc acetate dihydrate, aluminium chloride and diethanolamine (DEA) were used without any further purification. Ethyl alcohol was used as solvent after distillation.

2.2 Preparation

The undoped and Al doped ZnO thin films were prepared using sol–gel method onto glass substrates. For preparing undoped ZnO thin film, zinc acetate dihydrate was dissolved in a solution containing ethanol and diethanolamine (DEA). The molar ratio of DEA to zinc acetate was maintained as 1.0 and the concentration of zinc acetate was 0.5 M. Al doped ZnO film was prepared by adding aluminium chloride as a dopant in the precursor ZnO solution. The concentration of dopant was varied from 0.5 to 2 at. % in steps of 0.5 at. %. The prepared solutions were stirred for 1 h at 50 °C by a magnetic stirrer to yield a clear homogeneous solution. The obtained solution was allowed for aging at room temperature for 24 h before used for coating process. The final sol was used to prepare films using spin coating technique. First, glass substrates were immersed in chromic acid and then cleaned with soap solution followed by distilled water. After drying the glass plates, the prepared sol was dropped onto it and rotated at a constant speed of 2,500 rpm for 30 s using a spin coater. After each deposition, the film was dried at 150 °C for 10 min to remove the organic residuals. This process was repeated eight times to get the film of desired thickness. Finally, the film was annealed in air at 500 °C for 1 h.

2.3 Characterization techniques

The structural properties of ZnO:Al thin films were analyzed using X-ray powder diffraction (PANalytical-PW 340/60 X'pert PRO) technique with Cu–K α radiation ($\lambda = 1.5406 \text{ \AA}$). The optical and photoluminescence spectra of the thin films were observed using Perkin Elmer (Lambda 35) UV-vis-NIR spectrophotometer and spectrofluorometer (Perkin Elmer: FL Winlab LS 55 set up), respectively. The electrical conductivity of the thin films were determined using a phase sensitive multimeter (PSW – 1732) Newton 4th Ltd. (UK).

3 Results and discussion

3.1 Structural properties

The X-ray diffraction (XRD) patterns of all the AZO films prepared using spin coating technique and annealed in air

at 500 °C are shown in Fig. 1. Three prominent Bragg's diffraction peaks at the 2θ values of 30.0, 34.6 and 36.4 associated with (100), (002) and (101) planes, respectively were observed for the undoped ZnO thin films. These peaks are very narrow indicating the good crystallinity of undoped ZnO. The prepared ZnO:Al films exhibit hexagonal wurtzite structure with (002) as preferential orientation except the one with Al doping level of 2 at. %.

Even though, the preferential orientation is along (002) plane, the intensity of the peak related to this plane decreases gradually with the increase in the Al doping level up to 1.5 at. %, indicating a slight reorientation of the lattice planes with respect to the surface of the substrate [16]. This type of change in preferential orientation from (002) to some other planes has been reported by several researchers [17–19]. But, the Al doping levels at which the preferential orientation changes (critical doping level) is reported to be different by different researchers. This change over in the preferential orientation beyond the critical doping level may be attributed to the interstitial incorporation of excess Al³⁺ ions and/or the segregation of some other Al related phases around the grain boundaries [20].

Apart from ZnO characteristic peaks, no peaks that correspond to aluminium or any of its complex oxides are detected, which are normally expected to appear upon mixing these two materials. The presence of these possible secondary phases are not confirmed by XRD profiles because, the proportion of these compounds present in the product is not up to the detection limit of XRD technique.

The texture coefficient (TC) represents the texture of the film and is used to quantify the preferential orientation [21]. If the TC of a lattice plane is greater than unity, then the growth of the film is said to be preferentially along that plane.

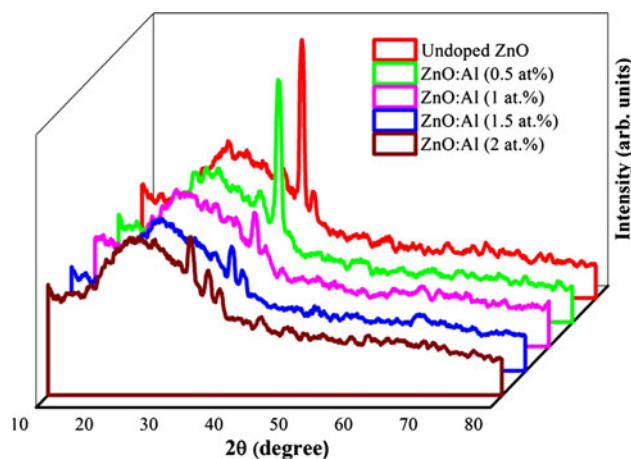


Fig. 1 XRD patterns of ZnO and ZnO:Al thin films

The TC of the AZO films is calculated using the relation [22]

$$TC_{(hkl)} = \frac{I_{(hkl)}/I_{0(hkl)}}{\frac{1}{N} \sum I_{(hkl)}/I_{0(hkl)}} \quad (1)$$

where $I_{(hkl)}$ is the observed intensity of the (hkl) plane, $I_{0(hkl)}$ is the standard intensity corresponds to the (hkl) plane taken from the JCPDS Data (Card No. 36-1451) and N is the number of diffraction peaks. The values of $TC_{(hkl)}$ are given in Table 1.

The undoped and doped films are found to have maximum texture coefficient for (002) plane except the one with Al doping level 2 at.%. This result clearly supports the predominance of (002) plane in all the undoped and doped ZnO films, except for the film prepared with highest doping level (2 at.%).

The crystallite size (D) is calculated using the Scherrer’s formula [23]

$$D = \frac{k\lambda}{\beta \cos \theta} \quad (2)$$

where k is a constant (0.9), λ is the wavelength of the incident X-ray ($\lambda = 1.54060 \text{ \AA}$), β is the corrected FWHM for instrumental broadening of the maximum intensity peak and θ is the angle at which the peak with maximum intensity occurs.

The obtained values of crystallite size are given in Table 2. It is seen that the crystallite size for Al doped films is less than that of the undoped ZnO film. This may be attributed to the change in the nucleation mechanism for the formation of ZnO films. As aluminium is doped, the number of nucleations for the formation of ZnO crystallites

enhances and results in a smaller crystallite size as a consequence [24]. This effect is more significant at a higher aluminium concentration.

Lattice constants a and c are calculated using the following well known analytical formulae [25].

$$a = \frac{\sqrt{1}}{\sqrt{3}} \frac{\lambda}{\sin \theta} \quad (3)$$

$$c = \frac{\lambda}{\sin \theta} \quad (4)$$

The calculated values of a , c and c/a ratio for the undoped and Al doped ZnO thin films are given in Table 2. The values of lattice constants are found to slightly vary with Al doping concentration. This indicates the tendency of structural modification promoted by the dopant Al on ZnO.

The peaks in the XRD pattern of undoped ZnO resulted in the lattice constant values, $a = 3.2392 \text{ \AA}$, $c = 5.1678 \text{ \AA}$ and $c/a = 1.5954$. The standard JCPDS data of ZnO having hexagonal wurtzite structure provides the lattice constant values as $a = 3.2498 \text{ \AA}$, $c = 5.2066 \text{ \AA}$ and $c/a = 1.6021$ (JCPDS Card No. 36-1451).

No significant change in the ratio of lattice parameters a and c is observed after doping. This confirms the point stated earlier that all Al ions are not substituted into the Zn sites but exist as interstitials in the vicinity of the oxygen vacancies and thus have prevented the lattice distortion of bare ZnO film [26, 27].

3.2 Optical properties

3.2.1 UV–vis–NIR transmittance studies

The transmittance spectra obtained for the AZO films are given in Fig. 2. The transmittance measurements reveal that the films are highly transparent in the visible region. Depending on the Al concentration in the starting solution, the transmittance value varies between 91 and 98 %. The transmittance of undoped ZnO film is 98 % and the value varies as the doping level increases and attains a lower value of 91 % for the maximum doping level of 2 at.%. The decrease in the visible transmittance may be due to the crystal defects generated by the incorporation of Al in the

Table 1 TC values of AZO thin films

Al doping level (at.%)	TC _(hkl)		
	(100)	(002)	(101)
0.0	–	6.25	0.02
0.5	0.03	6.25	–
1.0	–	6.25	–
1.5	–	6.25	1.86
2.0	4	2.01	0.11

Table 2 Structural and optical properties of ZnO:Al thin films

Al doping level (at.%)	Lattice constants in \AA			Crystallite size (D) in nm	Thickness (t) in nm	Optical band gap (E_g) in eV
	a	c	c/a			
0.0	3.2392	5.1678	1.5954	38.34	612	3.25
0.5	3.2437	5.1664	1.5927	36.32	634	3.41
1.0	3.2463	5.1652	1.5911	32.70	654	3.43
1.5	3.2486	5.1641	1.5896	27.97	678	3.47
2.0	3.2498	5.1620	1.5884	25.24	689	3.42

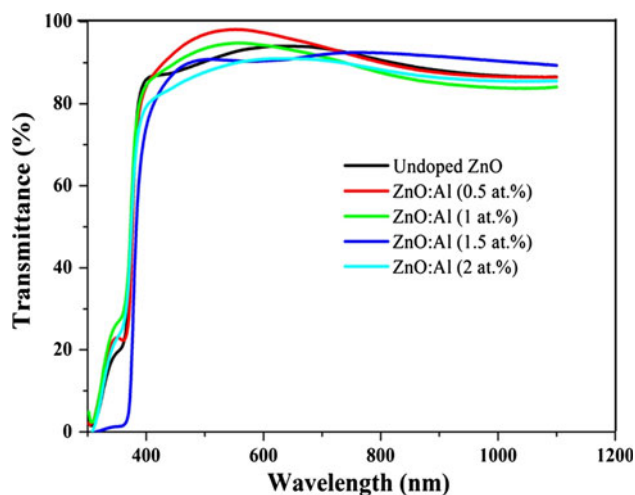


Fig. 2 Transmission spectra of ZnO:Al thin films

ZnO lattice. The transmittance in the near infrared region (NIR) is better for the AZO films with Al doping level of 1.5 at.% when compared with other films. It is important to mention here that the NIR transmission is significant, because increasing the long wavelength response is an approach to increase the efficiency of some solar cell devices as reported by Berginski et al. [28].

The absorption edge corresponds to the intrinsic band gap of ZnO. The detailed information about the band gap can be obtained by analyzing the dependence of absorption coefficient on photon energy in the high absorption regions.

The optical band gap (E_g) and absorption coefficient α are related by the equation

$$\alpha = (k/h\nu)(h\nu - E_g)^{n/2} \quad (5)$$

where ‘k’ is a constant, $h\nu$ the incident photon energy, ‘n’ a number that characterizes the nature of electronic transition between valance band and conduction band. For direct allowed transition $n = 1$ and it is well known that ZnO is a direct band gap semiconductor.

Therefore, Eq. (5) can be written as

$$\alpha = (k/h\nu)(h\nu - E_g)^{1/2} \quad (6)$$

The band gap energy of the undoped and Al doped ZnO thin films is determined by the extrapolation of the linear part of the plots [29] drawn for $(\alpha h\nu)^2$ against incident photon energy ($h\nu$) (not shown) and the obtained values of E_g are given in Table 2 along with the measured thickness.

In the present study, the band gap of undoped ZnO is determined as 3.25 eV and the value gradually increases with the increase in Al doping level up to 1.5 at.% and then decreased to 3.42 eV for the doping level of 2 at.%. The values of E_g are in good agreement with the band gap values of ZnO reported by earlier investigators [30, 31]. This variation in band gap is clearly reflected in the blue

shift of the absorption edge up to the doping level of 1.5 at.%, and the slight red shift in the case of 2 at.%.

The widening of optical band gap with Al doping is well described by Burstein–Moss effect [32]. By doping with Al, the aluminium atoms occupy the zinc sites in the ZnO lattice. Thus, at room temperature, they act as singly ionized donors giving one extra electron and these donated electrons occupy the states of the bottom of the conduction band, which results in a widening of the band gap as observed by Shrestha et al. [33].

Generally, band gap of thin films varies with film thickness, because of changes in barrier height at grain boundaries with thickness and also due to high density of dislocations and quantum size effect [34].

3.2.2 Photoluminescence studies

Photoluminescence spectra of undoped and Al doped ZnO thin films with different Al concentrations ranging from 0.5 to 2 at.%, annealed at 500 °C are shown in Fig. 3.

From the spectra, it can be seen that there is violet emission centered at 420 nm and blue–green emission centred at 493 nm.

Generally, ZnO exhibits a visible band centered at 510–540 nm (green emission) which is attributed to the oxygen vacancies (V_o^+) [35, 36]. It is seen in Fig. 3 that, the violet dominant emission of undoped ZnO thin film is subjected to blue shift for 0.5 at.% Al doped ZnO thin films followed by a red shift at 1 at.% Al doping. The shift was feeble for the other doping concentrations. The blue–green emission of undoped ZnO thin film observed at 493 nm has shown a significant blue shift (490 nm) only at 2 at.% of Al doping concentration.

These results may be connected with the change in the density of the defects like oxygen vacancies (V_o), zinc

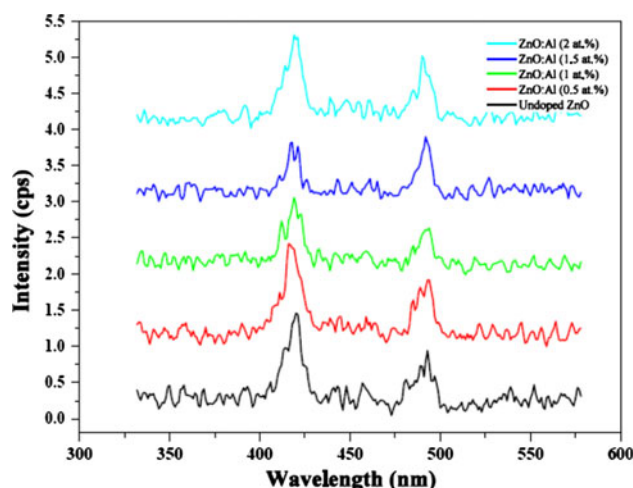


Fig. 3 PL spectra of undoped and Al doped ZnO thin films

vacancies (V_{Zn}), zinc interstitials (Zn_i), oxygen interstitials (O_i) and anti-site oxygen (O_{Zn}) [37].

The reason for the observed blue shift of the peak at 420 nm followed by a red shift can be discussed as follows: For Al doping concentration of 0.5 at.%, the number of Al substitutions is more than Al interstitials in the Al doped ZnO thin film. Considering charge equilibrium, the number of zinc vacancies (V_{Zn}^+) is larger than that of zinc interstitials (Zn_i). However, more zinc interstitials may be produced because of the increase in Al interstitials with increase in Al doping concentration. Change in the ratio of V_{Zn} to Zn_i results in a blue shift initially and then a red shift of the violet emission peak as Al doping concentration enhances from 0.5 to 2 at.% [38, 39].

3.3 Electrical properties

3.3.1 AC impedance studies of ZnO films

The AC impedance spectroscopy has been used to investigate the effect of the dopant Al^{3+} on the electrical conductivity of ZnO thin films because, the AC impedance spectroscopy can distinguish the conduction process in the grain and in the grain boundary.

Figure 4 shows the cole–cole plots for the impedance spectra of the undoped and doped ZnO specimens. All the spectra contain only a single arc. In general, independent of doping, the impedance spectra of semiconducting thin films are expected to exhibit two overlapping semicircle or arcs. The low frequency arc was interpreted as due to the grain boundary effect and the high frequency arc was attributed to the grain effect in the conventional view. The grain boundary effect on electrical conductivity may originate from a grain boundary potential barrier or from space

charge layers which are depleted in majority charge carriers and which are localized along the grain boundaries. However, a low frequency semicircle may also be an artifact caused by porosity, which is known as the constriction effect [40–42].

In the present work, the obtained single arc corresponding to low frequency is attributed to the grain boundary resistance. Some authors thought that [43, 44] the one arc spectrum means that the conduction process through the grain and the grain boundary had identical time constants, $\tau = 1/\omega = RC$, in which ω , R and C are peak frequency of the impedance arc, the resistance and the capacitance. This means that the conduction in the grain and the grain boundary occurs in the same process, so they cannot be separated by the impedance spectroscopy. Other authors thought that the single arc was interpreted as due to the contribution from the grain boundary based on the model having resistive grain boundaries and conducting grain cores [40, 43].

In common ZnO varistors or thin films, the grain boundary is several orders of magnitude and more resistive than the grain, so it is natural to attribute the impedance spectra completely to the response of the grain boundary and the contribution of the grain could be neglected [43].

In the present work also, the resistance values estimated from the cole–cole plot is of the order of $10^7 \Omega$ and hence it may be concluded that the calculated resistance values are of ZnO grain boundaries.

It is evident from the Fig. 4 that the addition of Al in various concentrations has altered the shape of impedance spectrum of undoped ZnO films. The grain boundary resistances estimated from the impedance plots are given in Table 3. The grain boundary resistance and hence conductivity are found to vary against the doping concentration of Al and is not showing any particular trend against the calculated grain size of ZnO and of Al concentration.

It is seen from the Table 3, that the grain boundary resistance values of all the Al doped ZnO films are lesser than that of bare undoped ZnO, though the doping content was very low as 0.5 at.%. This can be attributed to the fact that the trivalent Al ions increase the electrical conductivity

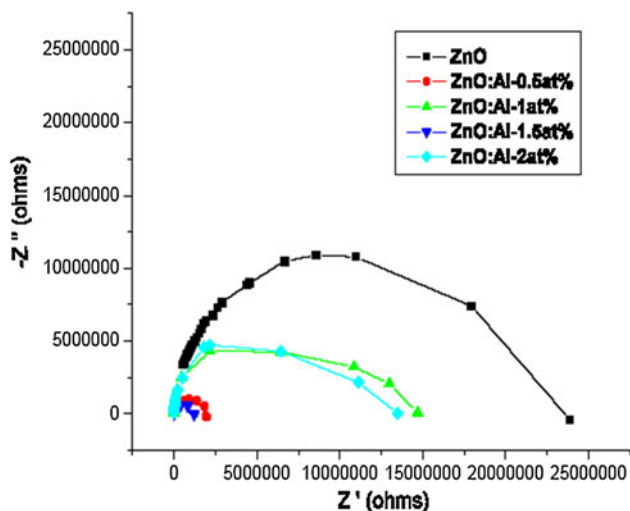


Fig. 4 Impedance spectra of AZO thin films for various doping concentrations at 0 V

Table 3 Grain boundary resistance of ZnO:Al thin films at various bias voltages

Al doping level (at.%)	Grain boundary resistance $\times 10^6$ in Ω			
	0 V	1 V	3 V	5 V
0.0	23.0	22.0	20.0	23.0
0.5	19.0	83.0	50.0	37.0
1.0	14.0	12.0	8.0	5.0
1.5	1.2	5.3	7.8	7.2
2.0	13.0	47.0	30.0	37.0

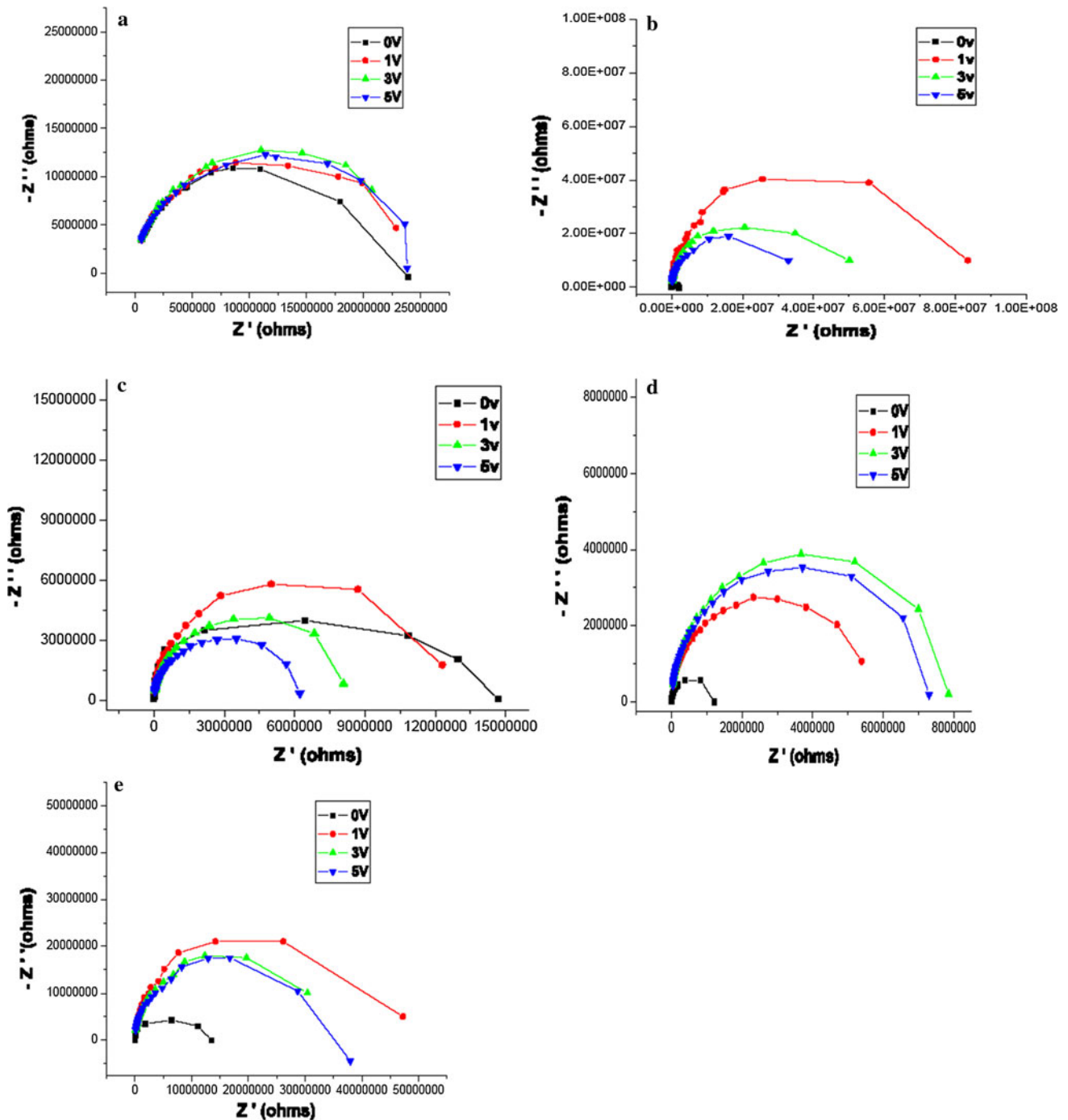


Fig. 5 **a** Impedance spectra of ZnO thin film at various bias voltages. **b** Impedance spectra of ZnO:Al (doping level 0.5 at.%) thin film at various bias voltages. **c** Impedance spectra of ZnO:Al (doping level 1 at.%) thin film at various bias voltages. **d** Impedance spectra of

ZnO:Al (doping level 1.5 at.%) thin film at various bias voltages. **e** Impedance spectra of ZnO:Al (doping level 2 at.%) thin film at various bias voltages

by forming a shallow donor in ZnO and hence reduce the grain boundary resistance [24].

When a small amount of aluminium is introduced in the solution of ZnO, Aluminium can play the role of an effective donor in ZnO layers, which can be explained by

the substitution introduction of Al^{3+} into the Zn^{2+} sites, generating free electrons [45].

Increase in the doping concentration of Al above 0.5 at.% has led to both increase and decrease of grain boundary resistance but the values are found to be lower

than that of bare undoped ZnO. This may be due to the changes in the number of substitutions of Al^{3+} ions in the Zn^{2+} sites and also the number of free electrons generated in ZnO. Jin et al. [39] have also observed the said effect for ZnO:Al thin films prepared using chemical spray pyrolysis method. Also, the decrease in the grain boundary resistance with increasing Al content suggests that a decrease in the distance between Al inclusion sites reduces the grain boundary resistance. The presence of Al solutes decreases the rates of densification and grain growth. The Al solutes may establish a depletion of the electrostatic barrier and hence fast electron transportation in ZnO films at higher Al concentration.

Impedance spectra drawn for various bias voltages 0, 1, 3 and 5 V for undoped ZnO and Al doped ZnO are given in above Fig. 5a–e for each concentration of Al. The calculated values of grain boundary resistance are given in Table 3.

The impedance spectra and the values of grain boundary resistance indicated the variation against the bias voltage. The asymmetric behavior of the arcs of impedance spectra changes with respect to applied bias voltage. This may be due to the change in the number of charge carriers from the ZnO grains that flow into the grain boundaries. The change in the charge carrier concentration not steadily increases or decreases with the increasing bias voltage.

In general, the trapping states within the interface layers are due to various metal oxide additions. There is a large quantity of mobile electrons in the n-type ZnO grains. The electrons tend to diffuse away to reach the interface layers and be trapped by the trapping states, leaving behind a positive fixed charge of ionized donors in the locality of the interface layers. Consequently, a depletion region is formed on both sides of the grain boundary and thus there are a series of schottky barrier diodes in the ZnO [46–48].

Therefore, the nature of the interface layer is of considerable interest, the knowledge of which plays an important role in understanding the highly non-ohmic property of the ZnO nanostructure.

The obtained values of grain boundary resistance for various bias voltages for undoped and Al doped ZnO films reveal that the films are non-ohmic in nature. It can also be stated that the non-ohmic nature of bare ZnO film has not been affected due to the Al doping.

Further, the variation of grain boundary resistance against the bias voltage may be ascribed to the variation of trap density of the samples [49].

4 Conclusion

The ZnO:Al thin films were prepared with the aluminium concentration varying from 0 to 2 at.%, increased in steps

of 0.5 at.% using the spin coating technique. All the films were annealed at 500 °C. The XRD studies revealed that the preferential orientation is found to be along the (002) plane for the undoped and Al doped ZnO films up to the doping level of 1.5 at.% and it changes in favour of (100) beyond that doping level. The structural studies also showed that the nucleation mechanism of ZnO has been influenced by the Al doping and the number of nucleation sites is found to be enhanced against the increase of Al doping concentration. This has resulted in the reduced crystallite size for the doped films.

It is inferred from optical study that the optical band gap was found to vary against the Al doping concentration in accordance with the Burstein–Moss effect. Photoluminescence study suggested that the blue shift and red shifts of violet emission is due to the change in the radiative centres between zinc vacancies and zinc interstitials caused by the increasing Al incorporation.

Variation in ZnO grain boundary resistance was observed through AC impedance study against Al doping concentration. It is attributed to the changing electrostatic barrier width at the grain boundaries established by the aluminium donor, against the aluminium concentration. Also, it was identified that the non-ohmic behavior of ZnO is not altered due to the Al doping.

References

1. L. Chinnappa, K. Ravichandran, K. Saravanakumar, G. Muruganatham, B. Sakthivel, *J. Mater. Sci. Mater. Electron.* **22**, 1827 (2011)
2. K. Saravanakumar, B. Sakthivel, K. Ravichandran, *Mater. Lett.* **65**, 2278 (2011)
3. S. Major, S. Kumar, M. Bhatnagar, K.L. Chopra, *Appl. Phys. Lett.* **49**, 394 (1986)
4. M. Vasanthi, K. Ravichandran, N. Jabena Begum, G. Muruganatham, S. Snega, A. Panneerselvam, P. Kavitha, *Superlattices Microstruct.* **55**, 180 (2013)
5. P. Ravikumar, K. Ravichandran, B. Sakthivel, N. Jabena Begum, A.T. Ravichandran, *J. Mater. Sci. Mater. Electron.* **24**, 4092 (2013)
6. S. Snega, K. Ravichandran, N. Jabena Begum, K. Thirumurugan, *J. Mater. Sci. Mater. Electron.* **24**, 135 (2013)
7. M.E.V. Costa, P.Q. Mantas, J.L. Baptista, *Sens. Actuators B Chem.* **27**, 312 (1995)
8. D. Scarano, S. Betarione, G. Spoto, A. Zecchina, C. Otero Areal, *Thin Solid Films* **400**, 50 (2001)
9. R. Anandhi, R. Mohan, K. Swaminathan, K. Ravichandran, *Superlattices Microstruct.* **51**, 680 (2012)
10. B. Ismail, M. Abaab, B. Rezig, *Thin Solid Films* **383**, 92 (2001)
11. J.W. Hoon, K.Y. Chan, J. Krishnasamy, T.Y. Tou, D. Knipp, *Appl. Surf. Sci.* **257**, 2508 (2011)
12. J.P. Kim, S.A. Lee, J.S. Bae, S.K. Park, U.C. Choi, C.R. Cho, *Thin Solid Films* **516**, 5223 (2008)
13. R. Chandramohan, V. Dhanasekaran, S. Ezhilvizhian, T.A. Vijayan, J. Thirumalai, A. John Peter, T. Mahalingam, *J. Mater. Sci.: Mater. Electron.* **23**, 390 (2012)

14. N. Jabena Begum, R. Mohan, K. Ravichandran, *Superlattices Microstruct.* **58**, 89 (2013)
15. H. Wang, M. Xu, J. Xu, M. Ren, L. Yang, *J. Mater. Sci.: Mater. Electron.* **21**, 589 (2010)
16. A.F. Aktaruzzaman, G.L. Sharma, L.K. Malhotra, *Thin Solid Films* **198**, 67 (1991)
17. C.M. Muiva, T.S. Sathiaraj, K. Maabong, *Ceram. Int.* **37**, 555 (2011)
18. B.J. Babu, A. Maldonado, S. Velumani, R. Asomoza, *Mater. Sci. Eng. B* **174**, 31 (2010)
19. L. Castaneda, R. Silva-Gonzalez, J.M. Gracia-Jimenez, M.E. Hernandez-Torres, M.A. Alejo, C.M. Beltran, M. de la, L. Olvera, J. Vega-Perez, A. Maldonado, *Mater. Sci. Semicond. Process.* **13**, 80 (2010)
20. K. Bahedi, M. Addou, M. El Jouad, Z. Sofiani, H. EL Ouzzani, B. Sahraoui, *Appl. Surf. Sci.* **257**, 8003 (2011)
21. R. Rajammal, K. Rajaram, E. Savarimuthu, S. Arumugam, *J. Nano-Electron. Phys.* **3**, 499 (2011)
22. K. Ravichandran, G. Muruganatham, K. Saravanakumar, S. Karnan, B. Kannan, R. Chandramohan, B. Sakthivel, *Surf. Eng.* **25**, 82 (2009)
23. V. Senthamilselvi, K. Saravanakumar, N. Jabena Begum, R. Anandhi, A.T. Ravichandran, B. Sakthivel, K. Ravichandran, *J. Mater. Sci. Mater. Electron.* **25**, 302 (2012)
24. S.T. Kuo, W.H. Tuan, J. Shieh, S.F. Wang, *J. Eur. Ceram. Soc.* **27**, 4521 (2007)
25. N. Shakthi, P.S. Gupta, *Appl. Phys. Res.* **2**, 19 (2010)
26. S.K. Kim, S.A. Kim, C.H. Lee, S.Y. Jeong, C.R. Cho, *Appl. Phys. Lett.* **85**, 419 (2004)
27. L.H. Xu, X.Y. Li, J. Yuan, *Superlattices Microstruct.* **44**, 276 (2008)
28. M. Berginski, J. Hupkes, A. Gordijin, W. Reetz, T. Watjen, B. Rech, M. Wuttig, *Sol. Energy Mater. Sol. Cells* **92**, 1037 (2008)
29. V. Senthamilselvi, K. Saravanakumar, R. Anandhi, A.T. Ravichandran, K. Ravichandran, *Optoelectronic. Adv. Mater. Rapid Commun.* **5**, 1072 (2011)
30. S.T. Tan, B.J. Chen, X.W. Sun, W.J. Fan, *J. Appl. Phys.* **98**, 013505 (2005)
31. B. Sundaresan, A. Vasumathi, K. Ravichandran, P. Ravikumar, B. Sakthivel, *Surf. Eng.* **28**, 323 (2012)
32. B.E. Sernelius, K.F. Berggren, Z.C. Jin, I. Hamberg, C. Granqvist, *Phys. Rev. B* **37**, 10244 (1988)
33. S.P. Shrestha, R. Ghimire, J.J. Nakarmi, Y.-S. Kim, S. Shrestha, C.-Y. Park, J.-H. Boo, *Bull. Korean Chem. Soc.* **31**, 112 (2010)
34. M. Pandiaraman, N. Soundararajan, C. Vijayan, *J. Ovonic Res.* **7**, 21 (2011)
35. J. Lü, K. Huang, J. Zhu, X. Chen, X. Song, Z. Sun, *Phys. B* **405**, 3167 (2010)
36. K. Vanheusden, W.L. Warren, C.H. Seager, *J. Appl. Phys.* **79**, 7983 (1996)
37. S. Zhao, Y. Zhou, K. Zhao, Z. Liu, P. Hun, S. Wang, W. Xiang, Z. Chen, H. Lu, B. Cheng, G. Yang, *Phys. B* **373**, 154 (2006)
38. X.L. Wu, G.G. Siu, C.L. Fu, *Appl. Phys. Lett.* **78**, 2285 (2001)
39. B.J. Jin, S. Im, S.Y. Lee, *Thin Solid Films* **366**, 107 (2000)
40. C.W. Nan, A. Tschöpe, S. Holten, H. Kliem, R. Birringer, *J. Appl. Phys.* **85**, 7735 (1999)
41. J.E. Bauerle, *J. Phys. Chem. Solids* **30**, 2657 (1969)
42. J. Fleig, J. Maier, *J. Electroceram.* **1**, 73 (1997)
43. Z. Zhou, K. Kato, T. Komaki, M. Yoshino, H. Yukawa, M. Morinaga, K. Morita, *J. Eur. Ceram. Soc.* **24**, 139 (2004)
44. J. Jose, M. Abdul, Kadhar, *Nanostruct. Mater.* **11**, 1091 (1999)
45. M. Ajili, N. Jebbari, N.K. Turki, M. Castagne, *International Renewable Energy Congress*, 305 (2010)
46. E. Elakrmi, R.B. Chaâbane, H.B. Ouada, *Akademia* **2**, 1 (2011)
47. R.N. Bhargava, D. Haranath, A. Mehta, *J. Phys. Soc.* **53**, 2847 (2008)
48. Y. Chen, R. Yua, Q. Shi, J. Qin, F. Zheng, *J. Mater. Lett.* **61**, 2551 (2007)
49. J. Zhang, L. Sun, J. Yin, H. Su, C. Liao, C. Yan, *Chem. Mater.* **14**, 4172 (2002)